ARTICLE

Unique white matter structural connectivity in early-stage drug-naive Parkinson disease

Virendra R. Mishra, PhD, Karthik R. Sreenivasan, MS, Zhengshi Yang, MS, Xiaowei Zhuang, MS, Dietmar Cordes, PhD, Zoltan Mari, MD, Irene Litvan, MD, Hubert H. Fernandez, MD, David Eidelberg, MD, Aaron Ritter, MD, Jeffrey L. Cummings, MD, DSc, and Ryan R. Walsh, MD, PhD

Neurology® 2020;94:e774-e784. doi:10.1212/WNL.0000000000008867

Correspondence
Dr. Mishra
mishrav@ccf.org
or Dr. Walsh
ryan.walsh@
barrowneuro.org

Abstract

Objective

To investigate the topographic arrangement and strength of whole-brain white matter (WM) structural connectivity in patients with early-stage drug-naive Parkinson disease (PD).

Methods

We employed a model-free data-driven approach for computing whole-brain WM topologic arrangement and connectivity strength between brain regions by utilizing diffusion MRI of 70 participants with early-stage drug-naive PD and 41 healthy controls. Subsequently, we generated a novel group-specific WM anatomical network by minimizing variance in anatomical connectivity of each group. Global WM connectivity strength and network measures were computed on this group-specific WM anatomical network and were compared between the groups. We tested correlations of these network measures with clinical measures in PD to assess their pathophysiologic relevance.

Results

PD-relevant cortical and subcortical regions were identified in the novel PD-specific WM anatomical network. Impaired modular organization accompanied by a correlation of network measures with multiple clinical variables in early PD were revealed. Furthermore, disease duration was negatively correlated with global connectivity strength of the PD-specific WM anatomical network.

Conclusion

By minimizing variance in anatomical connectivity, this study found the presence of a novel WM structural connectome in early PD that correlated with clinical symptoms, despite the lack of a priori analytic assumptions. This included the novel finding of increased structural connectivity between known PD-relevant brain regions. The current study provides a framework for further investigation of WM structural changes underlying the clinical and pathologic heterogeneity of PD.

From Imaging Research (V.R.M., K.R.S., Z.Y., X.Z., D.C.), Lou Ruvo Center for Brain Health (Z.M., A.R., J.L.C.), Cleveland Clinic Foundation, Las Vegas, NV; Departments of Psychology and Neuroscience (D.C.), University of Colorado at Boulder; Department of Neurosciences (I.L.), University of California San Diego, La Jolla; Center for Neurological Restoration (H.H.F.), Cleveland Clinic, OH; Center for Neurosciences (D.E.), Feinstein Institute for Medical Research, Manhasset, NY; UNLV Department of Brain Health (J.L.C.), School of Integrated Health Sciences, Las Vegas, NV; and Muhammad Ali Parkinson Center (R.R.W.), Barrow Neurological Institute, Phoenix, AZ.

Go to Neurology.org/N for full disclosures. Funding information and disclosures deemed relevant by the authors, if any, are provided at the end of the article.

Glossary

AD = Alzheimer disease; **DaT** = dopamine uptake transporter; **dMRI** = diffusion MRI; **FA** = fractional anisotropy; **FW** = free-water; **HC** = healthy controls; **Inf-Fron-Tri-Left** = left frontal inferior triangularis; **MDS-UPDRS-III** = Movement Disorder Society–sponsored Unified Parkinson's Disease Rating Scale Part III; **MNI** = Montreal Neurological Institute; **MoCA** = Montreal Cognitive Assessment; **NBS** = network-based statistic; **PALM** = permutation analysis of linear models; **PD** = Parkinson disease; **PPMI** = Parkinson's Progression Markers Initiative; **ROI** = region of interest; **SMA** = supplementary motor area; **WM** = white matter.

Neuroimaging studies suggest that Parkinson disease (PD) can be considered a network-disconnection syndrome,[1] which may be studied using network neuroscience approaches. Network neuroscience has broadly conceptualized the structures and functions of the brain as large-scale neural networks. It has been hypothesized that brain network dysfunction results from abnormalities in both anatomical connections and functional interactions of distributed brain regions.[2,3] Recent graph-theoretical findings[4,5] in early PD have suggested that although the functional modular organization of the PD connectome is disrupted, the structural organization of the PD connectome remains relatively preserved albeit with subtle white matter (WM) connectivity changes.[4] It is critical to understand whether the well-known inherent variability of anatomical networks[6,7] underlies the lack of detected structural disorganization in early PD. Furthermore, it is possible that the well-known pathologic and symptomatic heterogeneity of PD[8] affects the ability to detect consistent disease-relevant structural changes particularly early in the disease.

Generating a disease-relevant structural connectome, while minimizing the effect of inherent physiologic variance of anatomical networks and disease heterogeneity, is essential to improve understanding of structural network pathology in PD and enhance the reproducibility of structural network findings. In the current study, we utilized a novel whole-brain data-driven approach free from a priori assumptions that permitted focus on those connections that were most consistent across healthy controls (HC) and participants with early-stage PD to identify a group-specific WM anatomical network within both HC and PD. We hypothesized that a PD-specific WM anatomical network would explain structural network pathology including decreased structural connectivity between PD-relevant brain regions common across patients with PD (while enabling the preservation of individual structural anatomical variability) and would correlate with clinical markers as well as disease progression.

Methods

Participants

All data for this study were derived from the Parkinson's Progression Markers Initiative (PPMI) database, which is an observational multicenter study to identify PD biomarkers.[9] Diffusion MRI (dMRI) datasets acquired between 2011 and 2015 were downloaded in 2017 through a standard application process from the PPMI website (ppmi-info.org). Only the first available cardiac-gated dMRI scan with 2 repetitions for each participant was used in this study. Importantly, to minimize the noise characteristics from different scanners, only dMRI scans acquired using 3T Siemens (Munich, Germany) scanners were utilized in this study. These criteria yielded dMRI scans for a total of 92 participants with drug-naive PD and 49 HC that were further used for preprocessing and quality control.

Standard protocol approvals, registrations, and patient consents

The PPMI study was approved by the institutional review board of all participating sites, and written informed consent was obtained from all participants by the site investigators.

Participant characteristics

As described previously,[9] the primary inclusion criteria for all age-matched HC enrolled in the study were that the participants should be free of any observable neurologic deficits, have no first-degree family members with PD, and score 26 or greater on the Montreal Cognitive Assessment (MoCA).[10] The inclusion criteria for all participants with PD in the study were (1) diagnostic criteria for PD met; (2) diagnosed within 2 years of study enrollment; (3) an abnormal dopamine uptake transporter (DaT) scan documented; and (4) baseline Hoehn & Yahr scale score ≤2. A comprehensive baseline clinical evaluation of behavioral, cognitive, and motor assessments was performed for every participant by the site investigators. Motor severity score was calculated for each participant using the Movement Disorder Society–sponsored Unified Parkinson's Disease Rating Scale Part III (MDS-UPDRS-III).[11]

Image acquisition

The cardiac gated dMRI datasets used in the current study were acquired across 12 different scanning sites on 3T Siemens scanners with a 12-channel head coil. A 2D echoplanar diffusion sequence with the following measures was used at each site for every participant: number of diffusion encoding directions = 64, b-value = 1,000 s/mm^2, number of non-diffusion (b0) images = 1, number of repetitions = 2, matrix size = 112 × 112, slices = 72, in-plane resolution = 1.98 mm^2, slice thickness = 2 mm, flip angle = 90°, repetition time = 900 ms, and echo time = 88 ms.

In addition, DaT imaging was performed for all participants using SPECT. Briefly, data were acquired 4 ± 0.5 hours after

injection of 5 mCi of DaTscan. The imaging was performed with a 20% symmetric photopeak window centered on 159 KeV and 122 KeV with the following measures: matrix size = 128 × 128, number of projections = 120 or 90, step size = 3 or 4°. The uptake was calculated in bilateral caudate and putamen and was shared for all participants by the site investigators.

The details of the scanning measures are available at ppmi-info.org. Of note, the demographic and clinical variables of the participants' data were those recorded closest to the dMRI scan used in this study.

dMRI preprocessing and quality control

Each participant's dMRI scans were visually inspected for signal dropout or other artifacts before any preprocessing. After visual inspection, the dMRI scans were preprocessed in FSL using FMRIB software library version 5.0.9 (fmrib.ox.ac.uk/fsl/). To minimize the influence of diffusion-sensitizing gradients on dMRI volume, eddy current distortion correction was performed for each scan of every participant using eddy_correct in FSL. Each participant's movement in x, y, and z directions in every volume was computed based on the output of eddy_correct. Single tensor was then linearly fitted for every voxel inside the brain using dtifit, and fractional anisotropy (FA) was estimated in each voxel for every participant. A brain mask with a fractional intensity threshold of 0.2 was computed using bet before tensor-fitting to ensure the tensors were estimated only inside the brain voxels.

An estimate of total translational motion was calculated using the output file of eddy_correct. Briefly, the estimated translation motion in x, y, and z directions between each volume was summed across all the volumes by taking the root mean square motion of the 3 directions. Participants with mean +1*SD of diffusion motion greater than a voxel movement in the slice encoding direction were identified and removed from any further analysis. Rotation motion was not included in the quality control as rotations and translations are highly correlated during scanning.[12] This quality control process reduced the dMRI scans to a total of 70 participants with PD and 41 HC used for further analysis.

The table summarizes the clinical characteristics of all participants included in the current study.

Construction of structural connectome

Whole brain deterministic fiber tractography was conducted with an angle threshold of 35°[13] using TrackVis.[14] An FA mask of 0.2 and a length threshold of 10 mm[13] was applied to remove spurious white matter tracts. Resultant whole-brain connectivity provided the edges for building the structural connectome. The following steps were utilized to obtain the nodes in each participant's native space. First, the Montreal Neurological Institute (MNI) 152 template was registered to each participant's b0 image in native space using linear and nonlinear registration in FSL. Then, atlases from both automated anatomical labeling[15] with 90 anatomical regions of interest (ROIs) (no cerebellar regions) and ATAG[16] with 12 anatomical ROIs in the MNI 152 space were transformed to each participant's native space with nearest neighbor interpolation. The cortical and subcortical regions in each participant's native space thus obtained were treated as nodes.

A weighted structural connectivity matrix was then generated using the nodes and edges obtained for each participant. Two nodes (i, j) were said to be structurally connected if there was a WM fiber that had its endpoints in both nodes (i, j). Self-connectivity of a node was not utilized in this study. Structural connectivity was weighted by the product of the number of WM fibers (FN) generated using streamline tractography[17] between the 2 nodes, and average FA of these WM fibers to minimize the influence of noise in deterministic tractography. To further minimize the influence of noise, outlier detection was performed within each participant's connectivity matrix using the interquartile range[18] of the connectivity matrix.

Construction of group-specific WM anatomical network

To extract the most consistent cortical and subcortical connections across participants in each group, a nonparametric sign-test was conducted with Bonferroni correction ($p_{corr} < 0.05$) to identify group-specific WM anatomical connectivity[7] matrices in HC and PD. Importantly, the sign-test not only minimizes errors resulting from invalid streamline construction due to noise but also minimizes the false positivity inherent in deterministic tractography.[7] Both HC and PD-specific WM anatomical connectivity matrices thus obtained were used as masks to extract weighted structural connectivity matrices within each HC and PD participant. Graph-theoretical measures (described below) were then computed using these individual weighted structural connectivity matrices corresponding to the group-specific WM anatomical connectivity, and compared between groups to understand topologic differences of the group-specific WM anatomical connectivity.

Network topology analysis

Multiple global and local networks can be used to characterize the topology of a weighted network.[3] For the global network measure analysis, we focused on the small-worldness of group-specific WM anatomical connections to determine the efficiency of global integration and segregation of information flow between nodes of the network. Briefly, normalized path length (λ) can be used as a surrogate of global integration,[3] and normalized clustering coefficient (γ) can be used as a surrogate of global segregation.[3] Small-worldness (σ) in a network exists if $\lambda \approx 1$ and $\gamma \gg 1$, and suggests optimal information sharing between the local (γ) and distant neighbors (λ) of a node. We also computed network modularity,[19] which represents the hierarchy in the network structure.

For local network analysis, we focused on nodal efficiency and degree of the structural connectivity in each group. Briefly,

Table Participant demographics

Demographics	HC (n = 41)	PD (n = 70)	HC vs PD
Sex			NS (p = 0.64)
Female	14	27	
Male	27	43	
Handedness			NS (p = 0.46)
Left	4	6	
Right	32	60	
Mixed	5	4	
Age, y	62.12 ± 10.3	61.38 ± 10.11	NS (p = 0.69)
Years of education	15.68 ± 3.11	15.14 ± 2.98	NS (p = 0.4)
Disease duration, mo	NA	11.2 ± 12.69	NA
MDS-UPDRS-III	NA	20.04 ± 8.05	NA
MoCA score	28.17 ± 1.14	27.56 ± 1.88	NS (p = 0.19)
Hoehn & Yahr score (1/2)	NA	29/41	NA
Dominant affected side			NA
Left	NA	26	
Right	NA	43	
Mixed	NA	1	
Diffusion motion, mm	1.3 ± 0.4	1.32 ± 0.39	NS (p = 0.73)
Site			NS (p = 0.4)
1	2	6	
2	4	7	
3	1	2	
4	6	8	
5	2	5	
6	5	9	
7	1	7	
8	2	3	
9	5	9	
10	7	12	
11	5	0	
12	1	2	
Dopamine transporter scan score[a]	9.51 ± 1.81	5.3 ± 1.43	p < 0.001

Abbreviations: HC = healthy controls; MDS-UPDRS-III = Movement Disorder Society–sponsored Unified Parkinson's Disease Rating Scale Part III; MoCA = Montreal Cognitive Assessment; NA = not applicable; NS = nonsignificant; PD = Parkinson disease.
Values are reported as mean ±SD or n. Results of pairwise statistical comparisons are shown as p values.
[a] Dopamine transporter scan scores of caudate and putamen in both hemispheres were summed for each participant.

nodal efficiency characterizes the efficiency of information transfer of a node with the rest of the nodes in the network, both globally (nodal efficiency) and locally (nodal local efficiency). The nodal degree is the fundamental measure of the influence of a node in a network and nodes with a high degree have a significant effect on a network's information flow.[3] Nodal betweenness, in turn, characterizes the role of each node in information transfer in the network.[3]

The network measures computed in this study were compared between HC and participants with PD to understand whether there is a change in network topology in the WM structural connectivity of participants with early PD and to understand the correlation of these network measures with clinical measures.

Computation of participant-level connectivity score

We calculated overall connectivity strength by computing the summation of the inner dot product of the group-specific WM anatomical connectivity matrix (A) of each participant with PD, $\sum (A \times A^T)$, and we used this as a surrogate for a participant's connectivity score. We further tested whether the connectivity score was correlated with disease duration and severity.

Rich-club analysis

A rich-club organization is said to be present in a network when the hubs of a network tend to be more densely connected among themselves than with nodes with a lower degree. The presence or absence of a rich-club organization can provide insights into the higher-order modular structure of a network, thereby providing information about the network's resilience, hierarchical ordering, and specialization.[20] An increasing normalized coefficient Φnorm >1 over a range of nodal degree (k) was said to reflect the existence of a rich-club organization in a network.

Rich-club nodes, feeder nodes, and local nodes were identified for each participant using Φnorm for a given k, and the edges associated with these nodes were categorized into the rich-club, feeder, and local edges.[20] Feeder and local nodes are those nodes that either feed to rich-club nodes (feeder) or not (local). Since every participant within each group can have different nodes that can be identified as rich-club nodes, an upper threshold that yields at least one rich-club node in the group for a maximum k where the rich-club organization was evident within each group was computed empirically. A further constraint of the same threshold across the groups was applied to ensure there is no bias on this threshold.

Average rich-club edge strength, feeder edge strength, and local edge strength were then computed and compared between the groups to understand whether there is a difference in the rich-club structural organization in PD, and also whether edge strengths of the rich-club, feeder, and local nodes are associated with clinical measures.

All network measures were generated by using in-house MATLAB codes and GRETNA toolbox.[21] Figure 1 depicts the basic flow of the study.

Statistical analyses

Demographics and clinical variables

The χ^2 test was used to test the significance of categorical demographic variables and the Kruskal-Wallis test was used to determine the statistical significance of continuous demographic and clinical variables. Head motion during dMRI acquisition was compared using the nonparametric Kruskal-Wallis test. Statistical significance was established at $p < 0.05$ and the values were reported as mean ± SD for each demographic and clinical variable.

Comparison of group-specific WM structural connectomes

Network-based statistic (NBS)[22] was used to perform nonparametric statistical tests to identify whether there was a difference in WM structural connectivity between HC and PD. NBS performs permutation testing using unpaired *t* tests with 5,000 permutations. A test statistic was then computed for each connection, and a threshold of $t = 3.1$[22] was applied to identify a set of suprathreshold connections that showed significant differences ($p_{corr} < 0.05$) in group-specific WM anatomical connectivity between the groups.

Comparison of topographic network measures between HC and PD and correlation of network measures and clinical measures in PD

Nonparametric statistical analyses of group differences between global and local network properties, and their correlation with clinical variables, were conducted using the permutation analysis of linear models (PALM) toolbox in FSL.[23] Significance for PALM and NBS was established with family-wise error correction of $p_{corr} < 0.05$. All statistical comparisons in PALM and NBS were conducted with age, sex, handedness, years of education, total brain volume, site, and diffusion-motion measures as covariates of no interest.

Data availability

The anonymized data used in this study can be downloaded from the PPMI website and database.

Results

Demographics and clinical variables

The table summarizes the descriptive statistics for the demographics and clinical scores in participants with PD and HC.

None of the demographic characteristics, including sex, age, years of education, or handedness, was significantly different ($p > 0.05$) between the groups. Similarly, there was no significant difference between the groups ($p = 0.19$) in global cognition as assessed by MoCA. Patients with PD were early in the disease: mean disease duration was 11.2 ± 12.69 months, disease severity assessed by MDS-UPDRS-III score was 20.04 ± 8.05, and 29 and 41 participants with PD were identified to have Hoehn & Yahr scale scores of 1 and 2, respectively. As would be expected, there was a statistically significant difference ($p = 1.96 \times 10^{-17}$) in the cumulative DaT scan score between HC and patients with PD.

The mean head motion in HC and patients with PD during the dMRI scan was 1.3 ± 0.4 and 1.32 ± 0.39 mm, respectively, and was not found to be significantly different ($p = 0.73$).

Figure 1 Flowchart of the method

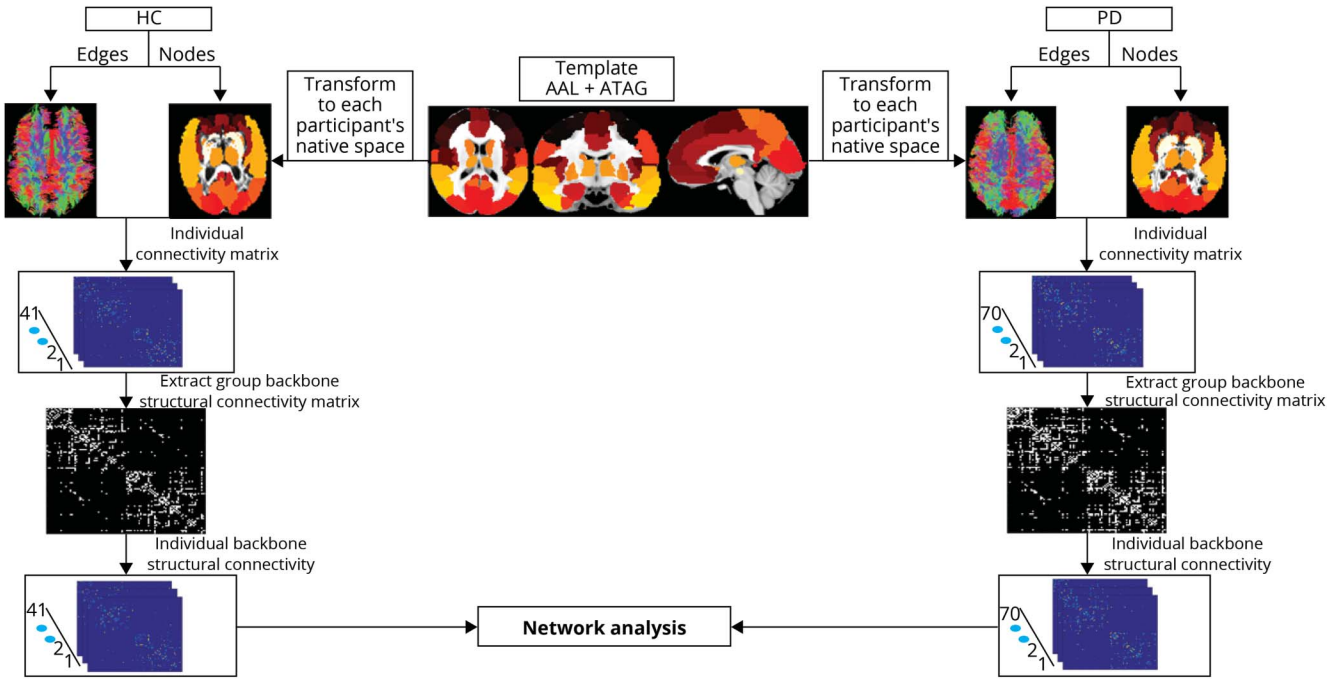

The combined automated anatomical labeling (AAL) and ATAG atlases were registered in each participant's native space to build the structural connectivity matrix. The edge-weight was computed as product of number of streamlines and average fractional anisotropy of streamlines between the nodes. Outlier detection was performed using interquartile range, and the weighted connectivity matrices were further utilized for each participant. A group backbone was computed for both healthy controls (HC) and patients with Parkinson disease (PD) using nonparametric sign test. Using the group backbone as the mask, network measures were computed for each participant at the backbone of the group.

Group-specific WM anatomical connectivity in HC and PD

Figure 2 shows a 3D representation of the group-specific WM structural connectivity. There were 864 and 1,220 edges (bilaterally) present in the WM structural connectivity of HC and participants with PD, respectively. As shown in figure 2A, there was 70.54% overlap in the structural connectivity of HC and participants with PD. There was only 1 connection (between olfactory and frontal orbital gyrus in the right hemisphere) that was found exclusively in HC-specific WM structural connectome (figure 2A), while 179/610 connections (figure 2A) involving cortical and subcortical regions such as precentral gyrus, insula, hippocampus, subthalamic nucleus, substantia nigra, and striatum were exclusively present in the PD-specific WM structural connectome.

Of note, NBS revealed 9 paths (figure 2B) involving angular gyrus, middle temporal gyrus, posterior cingulum, superior and middle occipital gyrus, caudate, putamen, striatum, supplementary motor area (SMA), precuneus, and frontal gyrus that were stronger in PD ($p_{corr} < 0.05$).

Topologic differences in group-specific WM connectivity between HC and PD

The global and local structural network properties of the 2 cohorts are depicted in figure 3. A significantly ($p_{corr} < 0.05$) impaired network architecture underlined by global weak information network transfer (figure 3A), accompanied by a significant ($p_{corr} < 0.05$) increase in nodal degree (figure 3B) of left frontal inferior triangularis (Inf-Fron-Tri-Left), was evident in the PD-specific WM connectome.

Correlation between global connectivity score and clinical measures in PD

There was a statistically significant ($p_{corr} < 0.05$) negative correlation between disease duration and global WM connectivity score in participants with PD, as shown in figure 4. There was, however, no correlation observed between the global connectivity score of participants with PD and disease severity or cumulative DaT score.

Correlation between graph-theoretical and clinical measures

No local or global network measures showed a correlation with any clinical variables for either group.

Differences in rich-club organization between group-specific WM connectomes

Both PD and HC-specific WM networks demonstrated the presence of a rich-club organization (figure 5A). A threshold of 80% was determined at the maximal nodal degree ($k \geq 9$) where both HC and PD had at least 1 node that can be classified as the network hub (rich-club node). This nodal degree was chosen to maximize the connections between the nodes

Figure 2 Group-specific white matter (WM) connectivity and network-based statistical (NBS) results

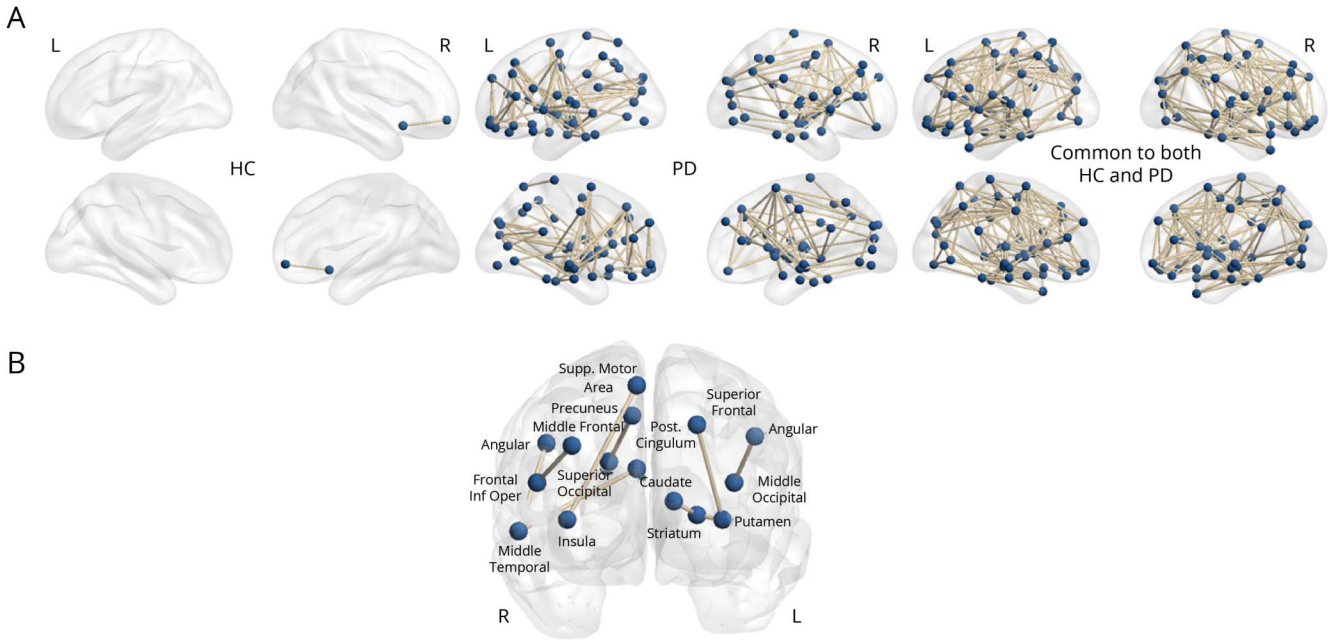

(A) Group-specific WM connectivity. Top panel shows the group-specific WM structural connectivity computed after Bonferroni correction at $p_{corr} < 0.05$. The paths that were exclusively present in the WM structural connectome of healthy controls (HC) and patients with Parkinson disease (PD), along with the paths that were present in both HC and patients with PD, are shown. Only 1 path between insula and middle frontal orbital gyrus in the right hemisphere was exclusively present in the HC-specific WM connectome. Several paths between cortical and subcortical regions such as precentral gyrus, insula, hippocampus, subthalamic nucleus, substantia nigra, and striatum were exclusively present in the PD-specific WM connectome. (B) NBS results. Paths with structural connectivity strength greater in patients with PD as compared to HC in group-specific WM structural connectome are shown. NBS paths were considered significant at $p_{corr} < 0.05$. R and L represent right and left hemispheres, respectively.

with the highest nodal degree. Three nodes (left hippocampus and bilateral insula) in HC and 6 nodes (bilateral insula, bilateral striatum, and bilateral hippocampus) in participants with PD were identified to be network hubs that had k ≥ 9 (figure 5A). Surprisingly, the WM connection strength between the network hubs (rich-club edges) (figure 5B) and WM connection strength feeding the network hubs (feeder edge strength [figure 5B]) exhibited a significantly ($p_{corr} < 0.05$) stronger connection in participants with PD as compared to HC. Although the WM connection strengths that were not connected to the hubs (local edge strength) did not reach adjusted statistical significance (figure 5B), the same trend was evident as was seen with rich-club edge strength and feeder edge strength.

Correlation between rich-club measures and clinical measures

Rich-club strength showed a significantly ($p_{corr} < 0.05$) positive correlation with MDS-UPDRS-III. Furthermore, feeder edge strength showed a significantly ($p_{corr} < 0.05$) positive correlation with cumulative DaT scan scores in PD (figure 6). No correlation was observed between any of the other rich-club measures and clinical observations in participants with PD.

Discussion

Our data-driven whole-brain proof-of-principle novel analytical approach, free from a priori assumption, utilizing dMRI from early-stage medication-naive PD in the PPMI database, identified the presence of a distinctive PD-specific structural connectome, along with the unanticipated novel finding of increased structural connectivity between known PD-relevant brain regions including striatum, caudate, putamen, and SMA. Some of the identified brain regions are classically thought to be involved in default-mode functional connectivity, while striatum, caudate, putamen, and SMA are integrally involved in the pathophysiology and motoric symptomatology in PD. These structural connectivity results, when taken together with recent functional connectivity data,[5,24,25] may suggest that structural connectivity changes constrain functional connectivity in early PD, resulting in a structurally fixed environment that may alter functional network capacity, and hence reduce functional network flexibility. Thus, our data support the hypothesis that structural network changes drive and constrain functional network capacity observed in early PD.

Despite the short time since diagnosis, mild disease severity, and disease heterogeneity of the participants with PD in the present investigation, our study was able to detect robust PD-specific structural connectivity that was correlated with disease duration, lending pathophysiologic credence to these data. In addition, the graph-theoretical measures derived using this PD-specific structural connectome correlated with disease duration, severity, and DaT deficiency, thereby further bolstering their pathophysiologic relevance, particularly in

Figure 3 Graph-theoretical measures in the white matter (WM) structural connectivity of Parkinson disease (PD)

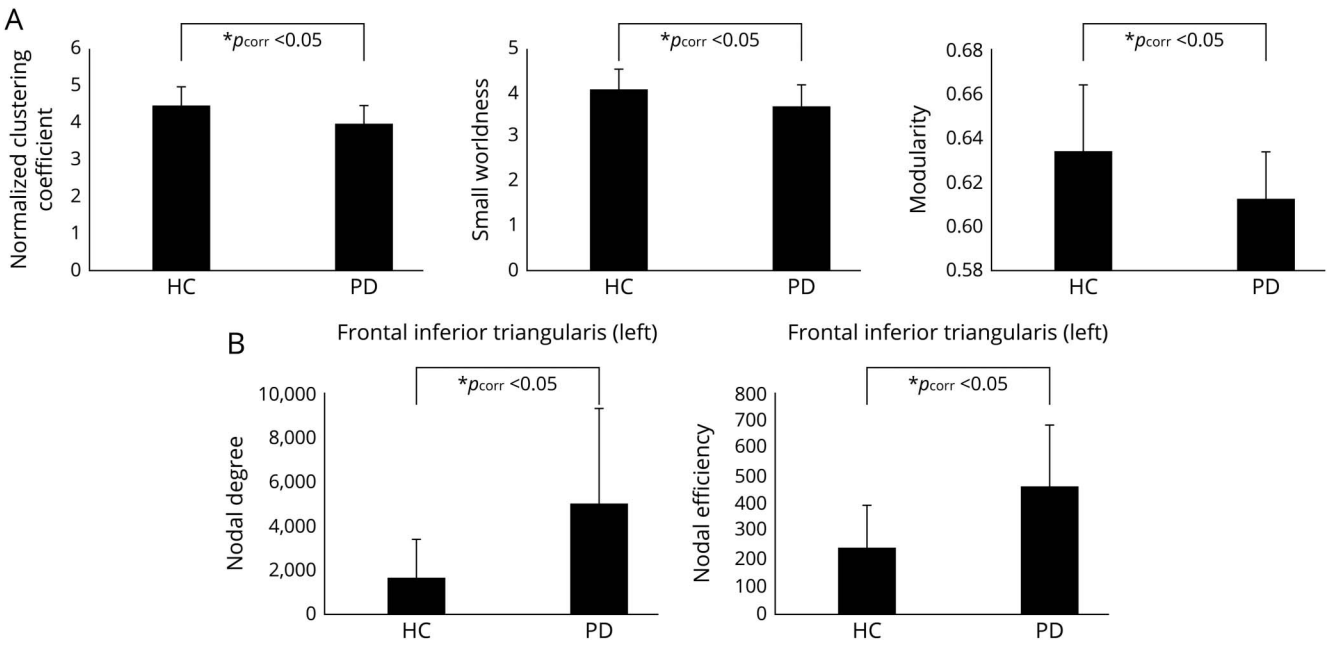

(A) Global graph-theoretical measures in the WM structural connectivity ofPD. Significantly lower normalized clustering coefficient, small-worldness, and modularity was observed in the WM structural connectome for PD, which are plotted as bar plots for both groups. (B) Local graph-theoretical measures in the WM structural connectivity of PD. Significantly higher nodal degree and nodal efficiency were observed in the left frontal inferior temporal lobe of PD. Furthermore, higher nodal degree and higher nodal local efficiency were observed in the left frontal inferior triangularis in the WM structural connectome for participants with PD and are plotted as bar plots for both groups. (A, B) Bar plots show the mean and the SD for each property within each group. HC = healthy controls.

light of the lack of a priori analytic assumptions. Overall, our study provides a baseline for future investigations of altered structural connectivity in PD given the early stage of disease in the PPMI cohort. Our study also suggests that the distinctive PD-specific anatomical connectivity may form the foundation for developing a diagnostic imaging biomarker to understand the association of altered structural connectivity with disease duration, development, and severity in PD.

In addition to involvement of several PD-specific regions such as subthalamic nucleus and striatum, it is intriguing that the connectivity pattern observed in PD-specific WM anatomical connectome consisted of various disease-independent regions such as hippocampus, precentral gyrus, and insula, which have been implicated in other neurodegenerative disorders such as Alzheimer disease (AD) and frontotemporal dementia. Incorporating these structural network changes, both at baseline and longitudinally, with widely reported functional network changes across various neurodegenerative diseases may provide important interventional targets to mitigate disease-specific functional network deficiencies.

Contrary to our hypothesis, we found an increase in nodal strength and local information transfer of Inf-Fron-Tri-Left. Both Inf-Fron-Tri-Left and angular gyri[26] are classically thought to be involved in semantic language processing, which is thought to be impaired in PD.[27] Also contrary to our hypothesis, both WM connection strength feeding the network hubs and WM connection strength between the network hubs demonstrated inverse correlations with clinical variables, suggesting that altered structural configuration in early-stage PD may be responsible for more rigid functional networks as revealed through both fMRI[24] and electrophysiologic data.[28] Alternatively, such increases in local network measures could

Figure 4 Relationship between disease duration and connectivity score derived using white matter (WM) structural connectome in Parkinson disease (PD)

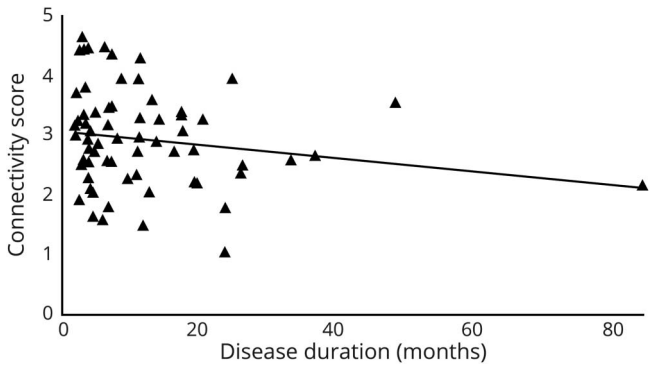

A significantly (p_{corr} < 0.05) negative correlation was observed between disease duration and structural connectivity score derived using the WM structural connectome in PD. Each scatterplot shows a connectivity score for each participant with PD. The slope was significant (p_{corr} < 0.05) and was established with family-wise error correction.

Figure 5 Rich-club measures

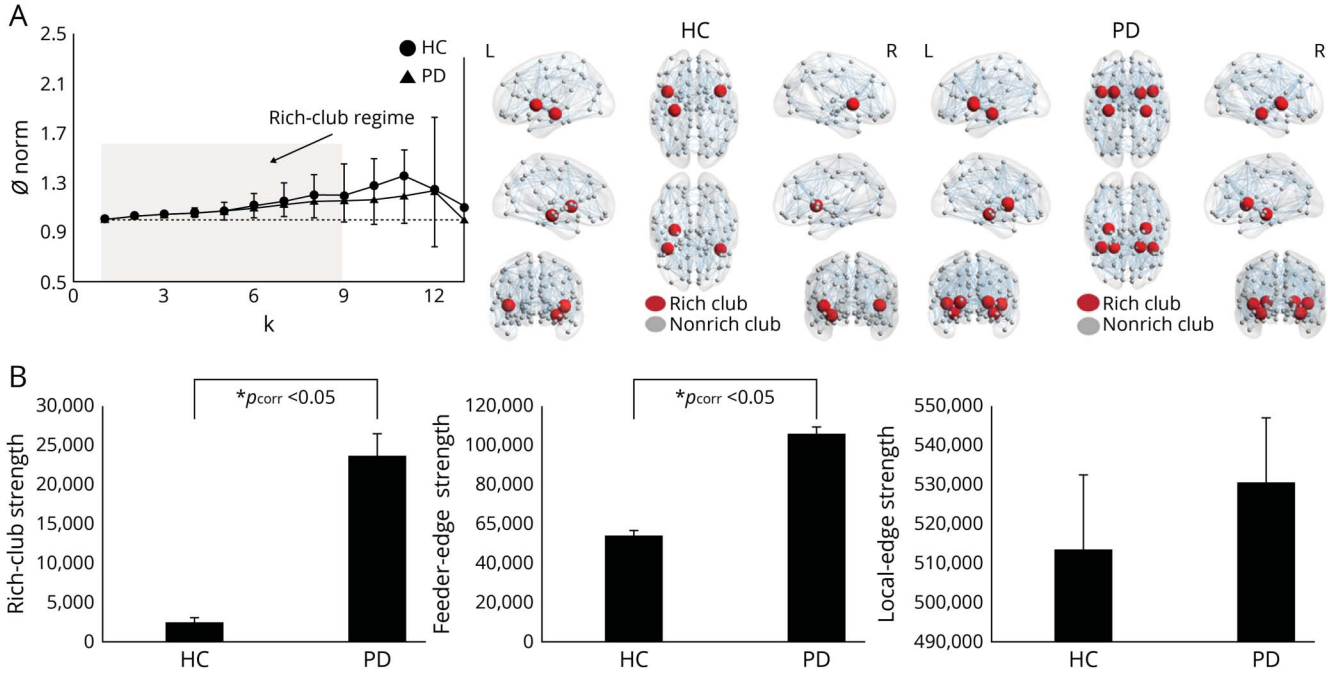

(A) Rich-club in the white matter (WM) structural connectome of healthy controls (HC) and patients with Parkinson disease (PD). Both HC and patients with PD showed the presence of rich-club from k ≥ 1 to k ≥ 9. The rich-club regimen is shown by the gray rectangle. The average Φ_{norm} is plotted against the degree (k) for both HC and patients with PD, shown as circles and triangles, respectively. The error bars indicate the deviation across the participants in each group. The rich-club nodes in both HC and patients with PD were extracted for k ≥ 9 and plotted on Montreal Neurological Institute152 template as red circles. The nodes identified to be non-rich-club are plotted as gray circles. (B) Differences in the rich-club measures between HC and patients with PD. Significantly higher rich-club strength (A) and feeder edge strength (B) were found in PD-specific WM structural connectome as compared to HC. Although differences in local edge strength did not reach corrected statistical significance, the same trend was evident as was seen for rich-club and feeder edge strength. Significance was established at $p_{corr} < 0.05$ using nonparametric statistical analysis.

represent a compensatory mechanism in early PD where these regions may selectively be hyperinvolved in information flow due to disconnection of neighboring nodes communicating with these selective nodes. Similar compensatory increases have been hypothesized in AD.[29] Further studies are needed, however, to understand the relationship between local information transfer and nodal strength with disease progression to further elucidate the role of these brain regions in the pathophysiology of PD.

Recent studies utilizing graph-theoretical approaches to dMRI in PD have reported conflicting findings, with some studies

Figure 6 Relationship between rich-club measures and clinical variables

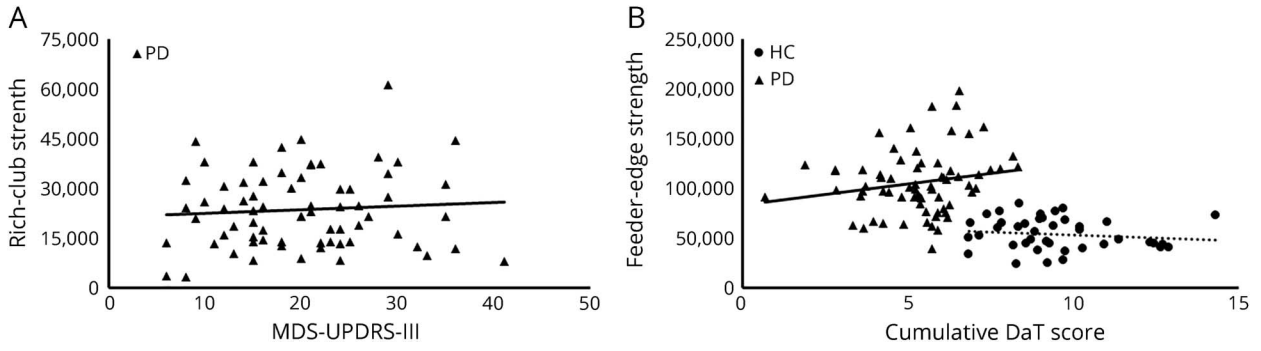

(A) Significantly ($p_{corr} < 0.05$) positive relationship was observed between rich-club strength and Movement Disorder Society–sponsored Unified Parkinson's Disease Rating Scale Part III (MDS-UPDRS-III). Furthermore, a significantly positive relationship between feeder edge strength and cumulative dopamine uptake transporter (DaT) score was observed for patients with Parkinson disease (PD), but not for healthy controls (HC). Scatterplot of both rich-club strength and feeder edge strength are plotted against (A) MDS-UPDRS-III and (B) cumulative DaT score, respectively, for patients with PD and HC. Each scatter represents the data from each participant. HC and patients with PD are represented as circles and triangles, respectively. Significance was established with family-wise error correction.

indicating weak information transfer,[30–32] and others not.[4,33] These findings may be affected by the choice of tracking algorithm (probabilistic or deterministic) and by the choice of edge weights, along with inherent anatomical heterogeneity among participants. While carefully controlling for anatomical variability, our findings were consistent with the reports of Nigro et al.[30] and Wen et al.,[33] suggesting that the discrepancies observed in dMRI-derived graph-theoretical measures may be guided by a lack of anatomical homogeneity between the participant groups more than the choice of edge weights used to build the structural connectome. PD-specific WM anatomical connectivity was found to depict impaired network architecture underlined by global weak information network transfer consistent with fMRI graph-theoretical findings of Tinaz et al.[4] However, Tinaz et al.[4] found no such difference using dMRI. This finding further suggests that care should be taken to remove the anatomical heterogeneity bias before performing graph-theoretical analysis using dMRI in PD.

A potential immediate clinical application of WM connectivity changes observed in this study involves the ability to compare changes in participant-specific anatomical connectivity by comparing participant-specific WM anatomical connectivity to PD-group-specific WM anatomical connectivity. This should further enable understanding of patient-specific structural changes, which is important to consider in this pathologically and phenotypically heterogeneous disease. Studies specifically powered to investigate this hypothesis are currently underway using multiple longitudinal PD cohorts, including across disease severity, symptom subscores, and cognitive impairment severity.

In an effort to avoid inappropriate inference due to potential for collinearity affecting the results, we restricted this initial proof-of-principle analysis to more global clinical measures (e.g., UPDRS-III without reference to specific subscores, disease duration). Because the PPMI data utilized herein (in our estimation) did not provide the necessary data to address such questions, we restricted our analyses to all participants with PD without subcharacterization to avoid overinterpretation and potential collinearity. Future studies will evaluate whether the differences observed in our study could be further differentiated among participants with PD with other clinical manifestations such as atypical parkinsonisms, PD with mild cognitive impairment, and PD with freezing of gait. A limitation in this study is that there was no statistically significant correlation ($p_{corr} <$ 0.42) observed after removing the participant with disease duration greater than 80 months (figure 4), although the negative correlation between disease duration and connectivity score was retained. This could be due to a loss in statistical power or an inherently weak correlation dependent on the outlier, and hence future studies should confirm this finding by including drug-naive patients with PD with disease duration between 40 and 80 months. In addition, we did not correct for free-water (FW) contamination[34] before fitting the tensors to obtain FA of the fibers. Future validation studies should estimate the influence of FW contamination in generating group-specific anatomical connectome. Since our study used imaging sites as a linear cofactor, which may not be ideal,[35] future studies should compare our findings to data collected at a single site on drug-naive participants with early-stage PD to evaluate the effects of scanner noise and other effects that may preclude observation of certain networks due to variable site-dependent noise characterization. Furthermore, simultaneous investigation of both functional and structural connectivity analysis employing this group-specific WM structural connectivity approach should shed light on the role of anatomical connectivity in modulating functional connectivity in PD.

By carefully minimizing variance in anatomical connectivity, this proof-of-concept whole-brain study free from a priori analytic assumptions on an early-stage PD cohort from a multisite database identified a number of PD pathologically relevant cortical and subcortical regions in the PD-specific WM connectome, which demonstrated a novel increase in structural connectivity when compared to HC, and was associated with impaired modular organization. By identifying a set of core abnormalities in early PD structural connectivity, this approach may permit improved ability to understand structural network–related disease progression and enhanced detection of changes in this core structural connectivity with disease-modifying therapies.

Acknowledgment

All authors had unrestricted access to the data in this study and had the final decision to submit for publication. The authors thank the participants of PPMI; Christopher Bird, who helped to download the data from the PPMI website to their local server for analysis; and Drs. Gaolang Gong and Yong He for discussions. Data used in the preparation of this article were obtained from the Parkinson's Progression Markers Initiative (PPMI) database (ppmi-info.org/data). For up-to-date information on the study, visit ppmi-info.org. PPMI, a public–private partnership, is funded by the Michael J. Fox Foundation for Parkinson's Research. Other funding partners include a consortium of industry players, nonprofit organizations, and private individuals, including AbbVie, Avid Radiopharmaceuticals, Biogen Idec, Bristol-Meyers Squibb, Covance, GE Healthcare, Genentech, GlaxoSmithKline, Eli Lilly and Company, Lundbeck, Merck, Meso Scale Discovery, Pfizer Inc., Piramal Imaging, Roche CNS Group, Servier, UCB, and Golub Capital.

Study funding

Funded by an Institutional Development Award (IDeA) from the National Institute of General Medical Sciences of the NIH (P20GM109025); and philanthropic funds from the Elaine P. Wynn and Family Foundation, Lynn and William Weidner Fund, The Sam and Peggy Grossman Family Foundation, The Samuel P. Mandell Foundation, The Peter and Angela Dal Pezzo funds, and The Keep Memory Alive (KMA) Young Scientist Award.

Disclosure

The authors report no disclosures relevant to the manuscript. Go to Neurology.org/N for full disclosures.

Publication history

Received by *Neurology* April 29, 2019. Accepted in final form August 28, 2019.

Appendix Authors

Name	Location	Role	Contribution
Virendra R. Mishra, PhD	Lou Ruvo Center for Brain Health, Cleveland Clinic Foundation, Las Vegas, NV	Author	Designing and conceptualizing the study, analyzing the data, drafting the manuscript for intellectual content
Karthik R. Sreenivasan, MS	Lou Ruvo Center for Brain Health, Cleveland Clinic Foundation, Las Vegas, NV	Author	Downloading and organizing the data, revising the manuscript
Zhengshi Yang, MS	Lou Ruvo Center for Brain Health, Cleveland Clinic Foundation, Las Vegas, NV	Author	Revising the manuscript
Xiaowei Zhuang, MS	Lou Ruvo Center for Brain Health, Cleveland Clinic Foundation, Las Vegas, NV	Author	Revising the manuscript
Dietmar Cordes, PhD	Lou Ruvo Center for Brain Health, Cleveland Clinic Foundation, Las Vegas, NV; University of Colorado at Boulder	Author	Revising the manuscript
Zoltan Mari, MD	Lou Ruvo Center for Brain Health, Cleveland Clinic Foundation, Las Vegas, NV	Author	Revising the manuscript
Irene Litvan, MD, FAAN	University of California San Diego, La Jolla	Author	Revising the manuscript
Hubert H. Fernandez, MD	Cleveland Clinic, OH	Author	Revising the manuscript
David Eidelberg, MD	Feinstein Institute for Medical Research, Manhasset, NY	Author	Revising the manuscript
Aaron Ritter, MD	Lou Ruvo Center for Brain Health, Cleveland Clinic Foundation, Las Vegas, Nevada	Author	Revising the manuscript
Jeffrey L. Cummings, MD, DSc, FAAN	UNLV Department of Brain Health, School of Integrated Health Sciences; Lou Ruvo Center for Brain Health, Cleveland Clinic Foundation, Las Vegas, NV	Author	Revising the manuscript
Ryan R. Walsh, MD, PhD, FAAN	Muhammad Ali Parkinson Center, Barrow Neurologic Institute, Phoenix, AZ	Author	Conceptualizing the study, analyzing the data, revising the manuscript

References

1. Cronin-Golomb A. Parkinson's disease as a disconnection syndrome. Neuropsychol Rev 2010;20:191–208.
2. Telesford QK, Simpson SL, Burdette JH, Hayasaka S, Laurienti PJ. The brain as a complex system: using network science as a tool for understanding the brain. Brain Connect 2011;1:295–308.
3. Rubinov M, Sporns O. Complex network measures of brain connectivity: uses and interpretations. Neuroimage 2010;52:1059–1069.
4. Tinaz S, Lauro PM, Ghosh P, Lungu C, Horovitz SG. Changes in functional organization and white matter integrity in the connectome in Parkinson's disease. Neuroimage Clin 2017;13:395–404.
5. Sreenivasan K, Mishra V, Bird C, et al. Altered functional network topology correlates with clinical measures in very early-stage, drug-naïve Parkinson's disease. Parkinsonism Relat Disord 2019;62:3–9.
6. Thompson PM, Schwartz C, Lin RT, Khan AA, Toga AW. Three-dimensional statistical analysis of sulcal variability in the human brain. J Neurosci 1996;16:4261–4274.
7. Gong G, He Y, Concha L, et al. Mapping anatomical connectivity patterns of human cerebral cortex using in vivo diffusion tensor imaging tractography. Cereb Cortex 2009;19:524–536.
8. Poewe W, Seppi K, Tanner CM, et al. Parkinson disease. Nat Rev Dis Primers 2017;3:17013.
9. Parkinson Progression Marker Initiative. The Parkinson Progression Marker Initiative (PPMI). Prog Neurobiol 2011;95:629–635.
10. Dalrymple-Alford JC, MacAskill MR, Nakas CT, et al. The MoCA: well-suited screen for cognitive impairment in Parkinson disease. Neurology 2010;75:1717–1725.
11. Goetz CG, Fahn S, Martinez-Martin P, et al. Movement Disorder Society–sponsored revision of the Unified Parkinson's Disease Rating Scale (MDS-UPDRS): process, format, and clinimetric testing plan. Mov Disord 2007;22:41–47.
12. Rae CL, Correia MM, Altena E, Hughes LE, Barker RA, Rowe JB. White matter pathology in Parkinson's disease: the effect of imaging protocol differences and relevance to executive function. Neuroimage 2012;62:1675–1684.
13. Cheng H, Wang Y, Sheng J, et al. Optimization of seed density in DTI tractography for structural networks. J Neurosci Methods 2012;203:264–272.
14. Wang R, Wedeen VJ. TrackVis.org. Proc Intl Soc Mag Reson Med 2007:3720.
15. Tzourio-Mazoyer N, Landeau B, Papathanassiou D, et al. Automated anatomical labeling of activations in SPM using a macroscopic anatomical parcellation of the MNI MRI single-subject brain. Neuroimage 2002;15:273–289.
16. Keuken MC, Bazin PL, Crown L, et al. Quantifying inter-individual anatomical variability in the subcortex using 7 T structural MRI. Neuroimage 2014;94:40–46.
17. O'Donnell LJ, Westin CF. An introduction to diffusion tensor image analysis. Neurosurg Clin N Am 2011;22:185–196, viii.
18. Rousseeuw PJ, Croux C. Alternatives to the median absolute deviation. J Am Stat Assoc 1993;88:1273–1283.
19. Newman MEJ. Modularity and community structure in networks. Proc Natl Acad Sci USA 2006;103:8577–8582.
20. van den Heuvel MP, Sporns O. Rich-club organization of the human connectome. J Neurosci 2011;31:15775–15786.
21. Wang J, Wang X, Xia M, Liao X, Evans A, He Y. GRETNA: a graph theoretical network analysis toolbox for imaging connectomics. Front Hum Neurosci 2015;9:386.
22. Zalesky A, Fornito A, Bullmore ET. Network-based statistic: identifying differences in brain networks. Neuroimage 2010;53:1197–1207.
23. Winkler AM, Ridgway GR, Webster MA, Smith SM, Nichols TE. Permutation inference for the general linear model. Neuroimage 2014;92:381–397.
24. Zhuang X, Walsh RR, Sreenivasan K, Yang Z, Mishra V, Cordes D. Incorporating spatial constraint in co-activation pattern analysis to explore the dynamics of resting-state networks: an application to Parkinson's disease. Neuroimage 2018;172:64–84.
25. Díez-Cirarda M, Strafella AP, Kim J, et al. Dynamic functional connectivity in Parkinson's disease patients with mild cognitive impairment and normal cognition. Neuroimage Clin 2018;17:847–855.
26. Seghier ML. The angular gyrus: multiple functions and multiple subdivisions. Neuroscientist 2013;19:43–61.
27. Cohen H. Language impairment in Parkinson's disease. In: Stemmer B, Whitaker HA, eds. Handbook of Neurolinguistics. San Diego: Academic Press; 1998:475–483.
28. Ellens DJ, Leventhal DK. Review: electrophysiology of basal ganglia and cortex in models of Parkinson disease. J Parkinson Dis 2013;3:241–254.
29. Bookheimer SY, Strojwas MH, Cohen MS, et al. Patterns of brain activation in people at risk for Alzheimer's disease. N Engl J Med 2000;343:450–456.
30. Nigro S, Riccelli R, Passamonti L, et al. Characterizing structural neural networks in de novo Parkinson disease patients using diffusion tensor imaging. Hum Brain Mapp 2016;37:4500–4510.
31. Kamagata K, Zalesky A, Hatano T, et al. Connectome analysis with diffusion MRI in idiopathic Parkinson's disease: evaluation using multi-shell, multi-tissue, constrained spherical deconvolution. Neuroimage Clin 2018;17:518–529.
32. Li C, Huang B, Zhang R, et al. Impaired topological architecture of brain structural networks in idiopathic Parkinson's disease: a DTI study. Brain Imaging Behav 2017;11:113–128.
33. Wen MC, Heng HSE, Hsu JL, et al. Structural connectome alterations in prodromal and de novo Parkinson's disease patients. Parkinsonism Relat Disord Engl 2017;45:21–27.
34. Burciu RG, Ofori E, Archer DB, et al. Progression marker of Parkinson's disease: a 4-year multi-site imaging study. Brain Engl 2017;140:2183–2192.
35. Mishra VR, Sreenivasan KR, Zhuang X, Yang Z, Cordes D, Walsh RR. Influence of analytic techniques on comparing DTI-derived measurements in early stage Parkinson's disease. Heliyon 2019;5:e01481.